

Chalmers Publication Library



This document is the Accepted Manuscript version of a Published Work that appeared in final form in *Journal of Physical Chemistry C*, copyright American Chemical Society after peer review and technical editing by the publisher. To access the final edited and published work see <http://dx.doi.org/10.1021/jp200751j>

(Article begins on next page)

A first-principles study of photo-induced water-splitting on Fe_2O_3

Anders Hellman^{*,†} and Raj G. S. Pala^{*,‡}

*Competence Centre for Catalysis and Department of Applied Physics, Chalmers University of
Technology SE-412 96 Göteborg, Sweden, and Department of Chemical Engineering, Indian
Institute of Technology, Kanpur 208016, India*

E-mail: ahell@chalmers.se; rpala@iitk.ac.in

*To whom correspondence should be addressed

†Competence Centre for Catalysis and Department of Applied Physics, Chalmers University of Technology SE-412
96 Göteborg, Sweden

‡Department of Chemical Engineering, Indian Institute of Technology, Kanpur 208016, India

Abstract

Photo-induced water-splitting on hematite (Fe_2O_3) is investigated by first-principles calculations. $(\text{HO})_3\text{-Fe-H}_3\text{O}_3\text{-R}$, $(\text{HO})_3\text{-Fe-O}_3\text{-R}$, $\text{O}_3\text{-Fe-O}_3\text{-R}$, $(\text{HO})_3\text{-Fe-R}$ and $\text{O}_3\text{-R}$ terminations are considered, where R represents the bulk stacking sequence. The stability under photoelectrochemical conditions and the free energy of all reaction intermediates in a simple one-electron transfer reaction mechanism is calculated and the ability of different surface terminations to function as a photo-anode is analyzed. Our results show that (i) under relevant photoelectrochemical conditions only $\text{O}_3\text{-Fe-O}_3\text{-R}$ and $\text{O}_3\text{-R}$ are stable and that (ii) the water-oxidation is only allowed on $(\text{HO})_3\text{-Fe-H}_3\text{O}_3\text{-R}$, $(\text{HO})_3\text{-Fe-O}_3\text{-R}$, $\text{O}_3\text{-Fe-O}_3\text{-R}$ from thermodynamic considerations. The results suggest that hematite, as long as the $(\text{HO})_3\text{-Fe-H}_3\text{O}_3\text{-R}$ termination is present under normal conditions, is a promising candidate for the photo-anode.

Introduction

To sustain society with sufficient energy without severely affecting the environment is a difficult challenge that needs to be resolved in the near future. Fortunately, several approaches are being evaluated¹ and photoelectrocatalysis, in which absorbed sunlight is converted to energy stored in chemical bonds, is one promising solution.^{2,3} Fujishima and Honda were able to show, using a TiO_2 -based photoelectrocatalyst, that photo-induced water-splitting is possible.⁴ However, the relatively large band-gap of TiO_2 , ~ 3.2 eV,⁵ limits the available part of the sunlight that can be harvested and used for the creation of electron-hole pairs. Due to the low efficiency of TiO_2 , many other materials have been investigated.^{6,7} For instance, hematite has a relatively small band-gap of ~ 2.1 eV,^{5,8,9} hence, should in principle, be able to harvest more sunlight. The theoretical limit of the conversion factor is as high as 12.9 %.⁵ Furthermore, as hematite is non-toxic, abundant and cheap, it has all the necessary properties for large scale applications of producing energy at a competitive price.^{9,10} However, measurements have never reported efficiencies close to the theoretical limit. The reason for the poor performance is ascribed to a number of effects, such as, low electron mobility,¹¹ rapid electron-hole pair recombination,¹² and slow surface reaction

kinetics.^{12,13} Besides, the position of the conduction band edge of Fe₂O₃ (~ 0.2 eV vs Normal Hydrogen Electrode) only allows the production of hydrogen if an external bias is applied.^{3,14}

Owing to their importance in technology, from corrosion to lubrication, magnetic materials, catalysis, and environmental processes, iron oxides have been the focus of much research.⁸ In surface science, hematite is the preferred model system for iron oxide, and thus has been characterized both by theory^{15–18} and experiment.^{19,20} As for the surface termination of Fe₂O₃, especially the (0001) facet, measurements conducted in ultra-high vacuum (UHV) indicate that both Fe- and O-termination coexist at different temperatures and O₂ partial pressures.¹⁹ These results are supported by theory as well.¹⁵ At higher oxygen pressures, the oxygen-termination becomes more stable.^{15,17,20} Under aqueous conditions, which are applicable to water-splitting, it is important to know how the interaction with water modifies the surface structure and composition, which would in turn affect the surface photoelectrochemistry. X-ray photoemission measurements of Fe₂O₃ in a humid environment show that the interaction with water depends on the existence of defects and the partial pressure of water.²¹ First-principles investigations^{15,18,22,23} show that even on a defect-free surface, hydroxylation of Fe₂O₃ is spontaneous. Using both theory and experiments, Trainor *et al.*¹⁸ provided strong evidence for the coexistence of two different hydroxylated surfaces, namely (OH)₃-Fe-H₃O₃-R and (OH)₃-R, which originate from Fe-terminated and O-terminated Fe₂O₃. Their results predict that the hydroxylated surfaces are considerably more stable than the dehydroxylated counterparts at high water pressures. This is supported by other recent X-ray photoemission measurements.²⁴

Recently Valdes *et al.*^{25,26} suggested a novel, theoretical framework in which the photo-oxidation of water can be described by first-principles methods. It is an extension of the electrochemical framework suggested by Rossmeis *et al.*^{25,27,28} Although the framework treats only the thermodynamics of the reaction mechanism, it provides a methodology for a detailed atomistic understanding of photoelectrochemical water-splitting. The framework assumed that the driving force for the reaction at the anode originates from the photo-induced hole at the edge of the valence band.^{25,26} Hence, in the scale obtained by aligning the energy levels of oxide semi-conductors

with the redox level of normal hydrogen electrode,² a deep valence band edge energy level will result in a larger thermodynamic driving force. Using the developed methodology, photoelectrochemical water oxidation has been addressed in TiO_2 ,²⁵ WO_3 ²⁶ and TiO_2 clusters.²⁹ Owing to the deeper valence band edge energy level in these systems, it was concluded that water-splitting is thermodynamically allowed for these oxide semiconductors, which is in agreement with experimental measurements. In comparison to the previous studies^{25,26,29} the valence band edge energy level in Fe_2O_3 is less deep,² and hence, it is possible that the water-splitting reaction on hematite is limited by its thermodynamics.

The aim of this article is to study the photo-oxidation of water on the $\text{Fe}_2\text{O}_3(0001)$ surface. To this end we utilize the first-principles methods to calculate the thermodynamics of reaction mechanisms involved in the photoelectrochemical oxidation of water. The reactions are assumed to occur on five different surface terminations of the $\text{Fe}_2\text{O}_3(0001)$ surface.

Computational methods and modeling methodology

The first-principles study is performed using the Density Functional Theory (DFT)^{30,31} as implemented in VASP.^{32–35} The Kohn-Sham orbitals are expanded using plane-waves with a kinetic energy cutoff of 450 eV. The projector augmented wave method^{36,37} is used to describe the interaction between valence electrons and the core. Six valence electrons for each O atom ($2s^2 2p^4$) and eight valence electrons for each Fe atom ($3d^7 4s^1$) are taken into account. The exchange-correlation is treated at the spin-polarized generalized-gradient approximation level by the use of the PBE functional.³⁸ An effective temperature of 0.1 eV is used to smear the Fermi discontinuity.

The hematite structure (space group $R\bar{3}c$) is described by a hexagonal unit cell that consists of six closed-packed hexagonal O layers and Fe ions that are placed in $2/3$ of the octahedral vacancies between the O layers.^{8,39} Using the nomenclature of Wang, *et al.*¹⁵ the unit cell can be represented by the repeat of six stoichiometric $-(\text{Fe-Fe-O}_3)-$ sequences. The bottom layer is terminated by the cleavage of the double Fe layer. The $\text{Fe}_2\text{O}_3(0001)$ surface is modelled in a slab geometry with a

(1x1) lateral periodicity. Four repeated Fe_2O_3 layers are used to describe the surface, of which the two top layers are allowed to relax. Henceforth, the atomic structure of the surface termination will be given explicitly, whereas the bulk stoichiometric sequence will be represented by -R. The slabs are separated by a vacuum distance of 15 Å. For the bulk and surface cells, the k-point sampling is performed with (8, 8, 2) and (5, 5, 1) Monkhorst-Pack grids,⁴⁰ respectively. The structural relaxations are performed within the quasi-Newton method, using the Hellmann-Feynman theorem for the force calculations. The ionic positions are optimized until the total residual force is less than 0.05 eV/Å.

In short, the theoretical framework by Valdes *et al.*^{25–28} can be summarized as: (i) the chemical potential of the $\text{H}^+ + \text{e}^-$ pair is related to that of $1/2 \text{H}_2$ in the gas-phase via the normal hydrogen electrode (NHE) at $U=0$,²⁷ (ii) the free energy of the reaction intermediates are calculated via DFT by also including the zero-point energy (ZPE) and vibrational contributions, (iii) the effect of bias on all states involving an electron in the electrode is included by shifting the reaction step by $-eU_{VB}$, where U_{VB} is the redox potential originating from the photo-induced hole in the valence band. As the band gap of hematite is estimated to be ~ 2.1 eV^{9,10} and the position of the conduction band edge is 0.2 eV versus NHE,^{3,14} the valence band edge is positioned at $U_{VB} \sim 2.3$ eV, (iv) the reference state are the energy of H_2 and H_2O in the gas-phase. The free energy change of the reaction step involving the formation of O_2 is set to the experimentally obtained value of 4.92 eV per O_2 molecule.⁴¹ Details regarding these approximations and their validity have been discussed extensively.^{25–28} Although activation barriers between the reaction steps might play an important role in the kinetics of photo-oxidation, these are not included in the model; instead the analysis is based on purely thermodynamic considerations. Thus, any discussion concerning kinetics is based on the minimum activation energy due to energy differences between the free energies of the different reaction steps. Furthermore, it should be noted that the position of the valence band depends on the pH according to $-k_B T \ln 10 \times \text{pH}$, however, the same dependence applies to the free energy of each reaction step for water oxidation. Thus, to a first approximation, the thermodynamics of the reaction is unchanged by changes in the pH.

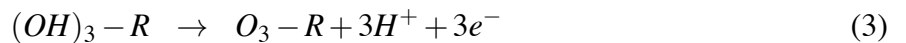
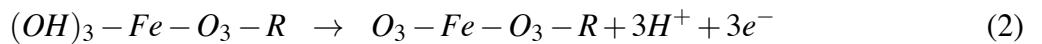
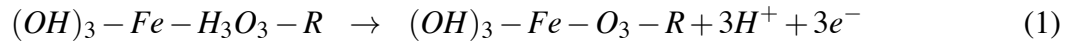
Results

In this section, results concerning surface termination under photoelectrochemical conditions, energy of reaction intermediates on the different surface terminations of $\text{Fe}_2\text{O}_3(0001)$ and the overall thermodynamics of photo-oxidation will be elaborated.

In consensus with recent studies,^{15,17} our calculations are restricted to the magnetic arrangement of an anti-ferromagnetic state with parallel spins inside the iron double layer. There is a good agreement between our calculated lattice parameters ($a=5.00 \text{ \AA}$ and $c=13.85 \text{ \AA}$) and other available first-principles calculations and experimental data.³⁹ To determine hematite's ability to function as a photo-anode material we will use the measured band gap of $\sim 2.1 \text{ eV}$.^{5,8,9}

Based on the study of Trainor et al,¹⁸ two surface terminations are considered to be most relevant, namely $(\text{OH})_3\text{-Fe-H}_3\text{O}_3\text{-R}$ and $(\text{OH})_3\text{-R}$, which are found to be particularly stable in the presence of water. However, under photoelectrochemical conditions, these terminations may become less stable as compared to more oxygen terminated surfaces.^{25,28,42} Thus, three more terminations, namely $(\text{OH})_3\text{-Fe-O}_3\text{-R}$, $\text{O}_3\text{-Fe-O}_3\text{-R}$ and $\text{O}_3\text{-R}$, will be used as model terminations for $\text{Fe}_2\text{O}_3(0001)$. In Figure 1, a top view of the considered terminations is given.

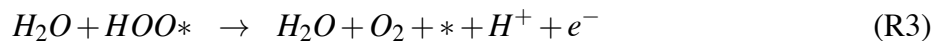
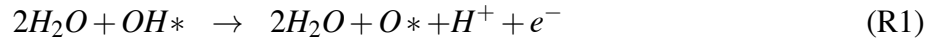
Under photoelectrochemical conditions, the stability of different surface terminations change owing to the redox potential, U_{VB} , generated by the photo-induced holes at the valence band. These holes can serve as electron acceptors and hence, promote electron generating disproportionation reactions like:



The relative stability of different surface terminations, calculated as the energy difference of the above reactions, are shown in Figure 2 at two different pH, namely, pH=0 and pH=14. It is clear that although the $(\text{OH})_3\text{-Fe-H}_3\text{O}_3\text{-R}$ and $(\text{OH})_3\text{-R}$ are the most stable terminations at zero potential,

none of these surfaces are stable under the photoelectrochemical conditions that apply for water-oxidation on $\text{Fe}_2\text{O}_3(0001)$, i.e., $U_{VB}=2.3$ eV. Instead, the highly oxidized surface terminations, $\text{O}_3\text{-Fe-O}_3\text{-R}$ and $\text{O}_3\text{-R}$ have the highest relative stability. Analyzing Figure 2 in greater detail, it is seen that at $\text{pH}=0$, the $\text{O}_3\text{-R}$ termination becomes the preferred one as compared to $(\text{OH})_3\text{-R}$ at a potential of $U=1.18$ eV, whereas $(\text{OH})_3\text{-Fe-O}_3\text{-R}$ and $\text{O}_3\text{-Fe-O}_3\text{-R}$ become the preferred termination as compared to $(\text{OH})_3\text{-Fe-H}_3\text{O}_3\text{-R}$ at a potential of $U=1.68$ V and $U=2.09$ V, respectively. At $\text{pH}=14$ the crossing between $\text{O}_3\text{-R}$ and $(\text{OH})_3\text{-R}$ occur at a potential of $U=0.35$ eV, while the transformation of $(\text{OH})_3\text{-Fe-H}_3\text{O}_3\text{-R}$ to $(\text{OH})_3\text{-Fe-O}_3\text{-R}$ and subsequently to $\text{O}_3\text{-Fe-O}_3\text{-R}$ occur at $U=0.86$ V and $U=1.06$ V, respectively. Although the relative stability clearly shows that only $\text{O}_3\text{-Fe-O}_3\text{-R}$ and $\text{O}_3\text{-R}$ terminations are relevant, the thermodynamic analysis of the water-oxidation was conducted on all surface terminations.

The reaction landscape of water-splitting depends on the surface termination. For the three hydroxylated terminations, $(\text{OH})_3\text{-Fe-O}_3\text{H}_3\text{-R}$, $(\text{OH})_3\text{-Fe-O}_3\text{-R}$ and $(\text{OH})_3\text{-R}$, the initial step in photo-oxidation is the activation of the OH-layer by the removal of a proton, followed by the splitting of a water molecule and formation of a surface OOH^* intermediate. O_2 originates from the OOH^* intermediate, and finally, splitting of a second water molecule completes the cycle. The reason for not considering a direct recombination of oxygen atoms to O_2 stems from the expectation of a large barrier for that particular process.⁴³ From the above, the following reaction scheme was put forth;



On the other hand, for the two oxygen terminated surfaces, $\text{O}_3\text{-Fe-O}_3\text{-R}$ and $\text{O}_3\text{-R}$, the initial

step in photo-oxidation is the splitting of a water molecule, thereby forming a surface OOH* intermediate, i.e., R2. This is followed by the O₂ removal from the OOH* intermediate, i.e., R3, and the splitting of a second water molecule, i.e., R4. Finally, the removal of a proton from the surface hydroxyl group, i.e., R1, completes the reaction cycle.

On the hydroxylated surface terminations, (OH)₃-Fe-H₃O₃-R, (OH)₃-Fe-O₃-R and (OH)₃-R, the change in free energy as described by the suggested reaction mechanism for photo-oxidation of water (see R1-R4) is calculated according to:

$$\Delta G_1 = \Delta E_1 + (\Delta ZPE + T\Delta S)_1 - eU_{VB} \quad (4)$$

$$\Delta G_2 = \Delta E_2 + (\Delta ZPE + T\Delta S)_2 - eU_{VB} \quad (5)$$

$$\Delta G_3 = \Delta E_3 + (\Delta ZPE + T\Delta S)_3 - eU_{VB} \quad (6)$$

$$\Delta G_4 = \Delta E_4 + (\Delta ZPE + T\Delta S)_4 - eU_{VB}. \quad (7)$$

The energetic contribution to each reaction step is presented in Table 1.

In this study, the interaction with the surrounding water molecules is not explicitly taken into account. There is a stabilization of OH* and OOH* owing to the polar nature of these reaction intermediates. Rossmeisl *et al.*²⁸ showed that depending on the hydrogen bonding geometries, the energy stabilization can range between 0.2 to 0.3 eV on Pt(111). Here, we assume that the average stabilization of OH* and OOH* is 0.25 eV.

Table 1: Reaction energies of the relevant reaction mechanism of water-splitting (see R1-R4)

	(OH) ₃ -Fe-H ₃ O ₃ -R	(OH) ₃ -Fe-O ₃ -R	O ₃ -Fe-O ₃ -R	(OH) ₃ -R	O ₃ -R
$\Delta E_1(E_{O^*}^i - E_{OH^*}^i + 1/2E_{H_2})$	1.212	1.455	1.747	0.930	0.967
$\Delta E_2(E_{OOH^*}^i - E_{O^*}^i + 1/2E_{H_2} - E_{H_2O})$	1.743	1.220	1.131	0.068	0.528
$\Delta E_3(E_*^i - E_{OOH^*}^i - 3/2E_{H_2} + 2E_{H_2O} + 4.92)$	1.996	0.652	1.020	3.233	3.118
$\Delta E_4(E_{OH^*}^i - E_*^i - E_{H_2O} + 1/2E_{H_2})$	-0.032	1.594	1.023	0.689	0.307

Vibrational modes and frequencies are determined by diagonalization of the Hessian matrix,

where the force derivatives are calculated by means of the central difference approximation with a displacement of 0.02 Å. From the frequencies, the zero-point energy (ZPE) and vibrational partition functions are determined. The entropy contributions (evaluated at T=298 K) for the different reaction intermediates are calculated using;

$$S = k_B \ln \prod_{i=1}^N \frac{1}{1 - \exp(-\hbar\omega_{X,i}/k_B T)} \quad (8)$$

where i is a specific vibrational mode and N is the total number of vibrational modes for reaction intermediate X . The gas-phase molecules are assumed to behave like an ideal gas with the appropriate translation and rotational contribution.⁴⁴ The calculated ZPE and entropy contributions are shown in Table 2.

Table 2: Zero-point energies and entropic contributions (evaluated at 298 K) to the free energies for all relevant reaction intermediates.

Intermediate	ZPE	TS
H ₂ O (0.035 bar)	0.580	0.67
H ₂	0.327	0.41
O ₂	0.097	0.64
O* (OH) ₃ -Fe-H ₃ O ₃ -R	0.077	0.02
OH* (OH) ₃ -Fe-H ₃ O ₃ -R	0.371	0.03
OOH* (OH) ₃ -Fe-H ₃ O ₃ -R	0.441	0.07
O* (OH) ₃ -Fe-O ₃ -R	0.062	0.04
OH* (OH) ₃ -Fe-O ₃ -R	0.386	0.02
OOH* (OH) ₃ -Fe-O ₃ -R	0.441	0.07
O* O ₃ -Fe-O ₃ -R	0.074	0.02
OH* O ₃ -Fe-O ₃ -R	0.328	0.06
OOH* O ₃ -Fe-O ₃ -R	0.442	0.06
O* (OH) ₃ -R	0.086	0.01
OH* (OH) ₃ -R	0.390	0.02
OOH* (OH) ₃ -R	0.448	0.06
O* O ₃ -R	0.073	0.02
OH* OH ₃ -R	0.384	0.03
OOH* OH ₃ -R	0.439	0.06

In Figure 3, the free energy of the photo-oxidation as calculated on a) (OH)₃-Fe-O₃H₃-R, b)

(OH)₃-Fe-O₃-R and c) (OH)₃-R is presented. In the case of (OH)₃-Fe-O₃H₃-R and (OH)₃-Fe-O₃-R terminations, the redox potential of the photo-induced hole is sufficient to make all reaction steps thermodynamically favorable. However, in the case of (OH)₃-R, it is clear that the photo-oxidation will be hindered by the stability of the OOH* reaction intermediate. There is at least a barrier of 0.75 eV that needs to be overcome for the photo-oxidation reaction to occur on this termination. It requires a U_{VB} of 3.1 eV before all reaction steps are thermodynamically allowed on the (OH)₃-R termination.

Figure 4 shows the free energy of photo-oxidation on O₃-Fe-O₃-R and O₃-R surface terminations. In the case of O₃-Fe-O₃-R, the redox potential of the photo-induced hole is sufficient to make all reaction steps thermodynamically favorable. In the O₃-R termination, it is clear that the photo-oxidation is prohibited by the strongly bound OOH* species. The thermodynamic barrier is calculated to be 0.65 eV. It requires a U_{VB} of 3.0 eV before all reaction steps are thermodynamically allowed on the O₃-R termination.

It should be noted that the one electron transfer reaction step, R3, need not be an elementary step and hence, might be further separated into non-electrochemical steps. After the proton is removed from the OOH* complex, the oxygen molecule needs to be desorbed from the active site. To evaluate the inclusion of non-electrochemical steps, we focused on the (OH)₃-Fe-O₃H₃-R and (OH)₃-R terminations. The desorption energy for the oxygen molecule in reaction step R3 was computed to be 0.72 eV and 2.03 eV for the surface terminations (OH)₃-Fe-O₃H₃-R and (OH)₃-R, respectively. Thus, including oxygen desorption in reaction R3 introduces a thermodynamically uphill step (Figure 3). However, assuming that O₂ desorption occurs in conjunction with water adsorption eliminates this particular thermodynamically uphill step on (OH)₃-R termination and shifts the rate-limiting step from R3 to R4. In the case of (OH)₃-Fe-O₃H₃-R termination, no thermodynamically uphill step is introduced by including the processes of desorption and adsorption into reaction step R3.

Discussion

From the stability analysis of the different terminations under photoelectrochemical conditions, it is clear that the photo-induced holes constitute a strong driving-force to break-up surface hydroxyl groups that are present in the solid-liquid interface. Thus, under steady-state conditions, only the completely oxygen-terminated surfaces should be present. However, at relatively high potentials in an electrochemical experiment, at least at low pH, the results also show that the hydroxyl-terminated surfaces can be stable, especially $(\text{OH})_3\text{-Fe-O}_3\text{H}_3\text{-R}$ and $(\text{OH})_3\text{-Fe-O}_3\text{-R}$. Besides, the hydroxyl-terminated surfaces can play an important role, (i) in the initial process of water oxidation on Fe_2O_3 before the production of photo-induced holes reaches steady-state, or (ii) if the water oxidation process is faster than the actual transport of holes to the surface.

Given the free energy landscapes for the photo-oxidation of water (Figure 3 and Figure 4), it is clear that the photo-induced hole at the valence band is thermodynamically just sufficient to make the reaction to occur spontaneously on the $(\text{OH})_3\text{-Fe-O}_3\text{H}_3\text{-R}$, $(\text{OH})_3\text{-Fe-O}_3\text{-R}$, $\text{O}_3\text{-Fe-O}_3\text{-R}$ terminations. This is in contrast to the two other terminations, $(\text{OH})_3\text{-Fe-R}$ and $\text{O}_3\text{-Fe-R}$, where the photo-oxidation is prohibited by at least 0.75 eV and 0.65 eV, respectively.

Owing to the modeling methodology, the analysis is restricted to energy differences between free energies of the different reaction steps. It is natural to assume that the reactions steps will be separated by activation barriers, which will further hinder the photo-oxidation reaction. This is especially important for the $(\text{OH})_3\text{-Fe-O}_3\text{H}_3\text{-R}$, $(\text{OH})_3\text{-Fe-O}_3\text{-R}$, $\text{O}_3\text{-Fe-O}_3\text{-R}$ terminations as the photo-oxidation is not thermodynamically hindered. However, the modeling of activation barriers in an electrochemical framework is difficult and this aspect remains as a future challenge.

Discrimination between electrochemical and non-electrochemical contributions of reaction step R3 shows that the desorption of the oxygen molecule is a difficult step. Hence, our results indicate that a destabilization of oxygen can be achieved for instance, by a change in pH, which will improve the thermodynamics on the $(\text{OH})_3\text{-R}$ terminations. The treatment of the non-electrochemical steps explicitly provides means to calibrate the effects of pH, which was unavailable in the novel modeling approach proposed by Valdes *et al.*^{25,26,29} However, if desorption occurs in conjunction

with water adsorption, there is a shift in the rate-determining step from R3 to R4 on $(\text{OH})_3\text{-R}$ terminations, whereas the conclusion that photo-oxidation is not hindered by thermodynamics on the $(\text{OH})_3\text{-Fe-O}_3\text{H}_3\text{-R}$ termination still holds.

If the photo-oxidation is hindered by slow surface-reaction kinetics, then there is a potential to improve the efficiency of the Fe_2O_3 by doping. In general, dopants may affect several aspects involved in photoelectrocatalysis, e.g., capture of photons, electronic conductivity, separation of electron-hole pairs, surface reaction kinetics, and the thermodynamics of reaction intermediates.^{9,45} It is generally known that dopants affect the surface chemistry in heterogeneous catalysis.⁴⁶ The present approach towards treating the non-electrochemical steps provides a method to calibrate the effect of dopants on surface chemistry in the context of photoelectrochemical systems. This is an interesting point that will be investigated in the near future.

There is one serious issue that remains to be elucidated. The two hydroxylated surface terminations that have been considered in this study have been shown to be the most stable ones in an aqueous environment.¹⁸ However, the stability of these terminations with respect to aqueous Fe^{3+} or solution pH was not considered and can potentially have a large impact on the reaction thermodynamics.¹⁸ This is an issue that requires future attention, however, it lies outside the scope of this study.

Conclusions

The photo-oxidation of water on $\text{Fe}_2\text{O}_3(0001)$ was investigated using first-principles calculations. Three different hydroxylated terminations, namely $(\text{OH})_3\text{-Fe-O}_3\text{H}_3\text{-R}$, $(\text{OH})_3\text{-Fe-O}_3\text{-R}$ and $(\text{OH})_3\text{-Fe-R}$, together with two oxygen-terminated surfaces, namely, $\text{O}_3\text{-Fe-O}_3\text{-R}$ and $\text{O}_3\text{-Fe-R}$, were explored. Under photoelectrochemical conditions, only the oxygen-terminated surfaces, $\text{O}_3\text{-Fe-O}_3\text{-R}$ and $\text{O}_3\text{-Fe-R}$, were found to be stable. The calculated free energy landscape showed that photo-induced water-splitting can occur spontaneously on the $(\text{OH})_3\text{-Fe-O}_3\text{H}_3\text{-R}$, $(\text{OH})_3\text{-Fe-O}_3\text{-R}$ and $\text{O}_3\text{-Fe-O}_3\text{-R}$ terminations, whereas the water oxidation reaction on both $(\text{OH})_3\text{-Fe-R}$ and $\text{O}_3\text{-Fe-R}$

was prohibited from a thermodynamics perspective. These results suggest that hematite, as long as the $(\text{HO})_3\text{-Fe-H}_3\text{O}_3\text{-R}$ termination is present under normal conditions, it will reconstruct to the $\text{O}_3\text{-Fe-O}_3\text{-R}$ termination under photoelectrochemical conditions, which in turn is a promising candidate for the photo-anode.

Acknowledgments

We thank Prof. Eric McFarland for valuable discussions. The calculations were performed at Neolith (Linköping). Support from the Swedish Research Council is acknowledged.

Appendix

An important issue that is not dealt with in our analysis of hematite's ability to operate as a photocatalyst is the fact that the Fe d electrons in hematite are considered to be strongly correlated. For certain optical properties, such as the band-gap, this is a critical issue. One way to treat correlated systems is to use DFT+ U in which the on-site Coulomb repulsion is described by a Hubbard parameter U , which is correlated to the energy required to add an extra d electron to the Fe atom, and a parameter J that is correlated to the screened exchange energy. Rollmann *et al.*¹⁶ showed that good agreement in band-gap between theory and experiment can be achieved by going beyond ordinary DFT, i.e. using a DFT+ U method. Rollmann *et al.* proposed that using $U=4$ eV will give the best overall agreement with experiments. However, Barbier *et al.*²⁰ recently presented strong evidence that ordinary DFT described the surface terminations of hematite better as compared to DFT+ U . It was suggested that U can vary from the bulk to the surface and from one termination to the next.

To assess the importance of the parameter U , we have evaluated the free energies of reactions R1-R4 by varying U between 1 to 5 (where 1 is ordinary DFT). In our calculations, J is kept at constant value of $J = 1$ eV. For further details, and additional see ref.¹⁶ We focused only on the $(\text{OH})_3\text{-Fe-O}_3\text{H}_3\text{-R}$ termination and calculated the energetics of the different reaction intermediates

as as a function of U (Figure 5). Although there is a stabilization of R3 as compared to the other reaction intermediates for low U values, and this does not affect the overall conclusions. Only at high values of U , there is a crossing of the lines (indicating a thermodynamic constraint on photo-oxidation), which affects our results and consequently our conclusions. However, such high values are in not in agreement with studies on surface terminations of hematite.²⁰

References

- (1) Dresselhaus, M. S.; Thomas, I. L. *Nature* **2001**, *414*, 332.
- (2) Grätzel, M. *Nature* **2001**, *414*, 338.
- (3) Bak, T.; Nowotny, J.; Rekas, M.; Sorrell, C. C. *Int. J. Hydrogen Energy* **2002**, *27*, 991.
- (4) Fujishima, A.; Honda, K. *Nature* **1972**, *238*, 37.
- (5) Murphy, A.; Barnes, P.; Randeniya, L.; Plumb, I.; Grey, I.; Horne, M.; Glasscock, J. *Int. J. Hydrogen Energy* **2006**, *31*, 1999.
- (6) Zou, Z.; Ye, J.; Sayama, K.; Arakawa, H. *Nature* **2001**, *414*, 625.
- (7) Nowotny, J.; Sorrell, C. C.; Sheppard, L. R.; Bak, T. *Int. J. Hydrogen Energy* **2005**, *30*, 521.
- (8) Cornell, R.; Schwertmann, U. *The iron oxides: Structure, Properties, Reactions, Occurrences, and Uses*; Wiley-Vch Weinheim, 2003.
- (9) Kleiman-Shwarsstein, A.; Hu, Y.-S.; Forman, A. J.; Stucky, G. D.; McFarland, E. W. *J. Phys. Chem. C* **2008**, *112*, 15900.
- (10) Glasscock, J. A.; Barnes, P. R. F.; Plumb, I. C.; Savvides, N. *J. Phys. Chem. C* **2007**, *111*, 16477.
- (11) Rosso, K. M.; Smith, D. M. A.; Dupuis, M. *J. Chem. Phys.* **2003**, *118*, 6455.
- (12) Ahmed, S. M.; Leduc, J.; Haller, S. *J. Phys. Chem.* **1988**, *92*, 6655.

- (13) Dareedwards, M. P.; Goodenough, J. B.; Hamnett, A.; Trelvellick, P. R. *J. Vhem. Soc. Faraday Trans. I* **1983**, *79*, 2027.
- (14) Sanchez, C.; Sieber, K. D.; Somorjai, G. A. *J. Electroanal. Chem.* **1988**, *252*, 269.
- (15) Wang, X.-G.; Weiss, W.; Shaikhutdinov, S. K.; Ritter, M.; Petersen, M.; Wagner, F.; Schlögel, R.; Scheffler, M. *Phys. Rev. Lett* **1998**, *81*, 1038.
- (16) Rollmann, G.; Rohrbach, A.; Entel, P.; Hafner, J. *Phys. Rev. B* **2004**, *69*, 165107.
- (17) Bergermayer, W.; Schweiger, H. *Phys. Rev. B* **2004**, *69*, 195409.
- (18) Trainor, T. P.; Chaka, A. M.; Eng, P. J.; Newville, M.; Waychunas, G. A.; Catalano, J. G.; BrownJr., G. E. *Surf. Sci.* **2004**, *573*, 204.
- (19) Thevuthasan, S.; Kim, Y. J.; Yi, S. I.; Chambers, S. A.; Morais, J.; Denecke, R.; Fadley, C. S.; Liu, P.; Kendelewicz, T.; BrownJr., G. E. *Surf. Sci.* **1994**, *425*, 276.
- (20) Barbier, A.; Stierle, A.; Kasper, N.; Guittet, M. J.; Jupille, J. *Phys. Rev. B* **2007**, *75*, 233406.
- (21) Liu, P.; Kendelwicz, T.; Jr., G. E. B.; Nelson, E. J.; Chambers, S. A. *Surf. Sci.* **1998**, *417*, 53.
- (22) Yin, S.; Ma, X.; Ellis, D. E. *Surf. Sci.* **2007**, *601*, 2426.
- (23) Yin, S.; Ellis, D. E. *Surf. Sci.* **2008**, *602*, 2047.
- (24) Yamamoto, S.; Kendelewicz, T.; Newberg, J. T.; Ketteler, G.; Starr, D. E.; Mysak, E. R.; Andersson, K. J.; Ogasawara, H.; Bluhm, H.; Salmeron, M.; Jr., G. E. B.; Nilsson, A. *J. Phys. Chem. C* **2010**, *114*, 2256.
- (25) Valdes, A.; Qu, Z.-W.; Kroes, G.-J.; Rossmeisl, J.; Norskov, J. K. *J. Phys. Chem. C* **2008**, *112*, 9872.
- (26) Valdes, A.; Kroes, G.-J. *J. Chem. Phys.* **2009**, *130*, 114701.

- (27) Norskov, J.; Rossmeisl, J.; Logadottir, A.; Lindqvist, L.; Kitchin, J. R.; Bligaard, T.; Jónsson, H. *J. Phys. Chem. B* **2004**, *108*, 17886.
- (28) Rossmeisl, J.; Logadottir, A.; Norskov, J. K. *Chem. Phys.* **2005**, *319*, 178.
- (29) Valdes, A.; Kroes, G.-J. *J. Phys. Chem C* **2010**, *114*, 1701.
- (30) Hohenberg, P.; Kohn, W. *Phys. Rev.* **1964**, *136*, B864.
- (31) Kohn, W.; Sham, L. J. *Phys. Rev.* **1965**, *140*, A1133.
- (32) Kresse, G.; Hafner, J. *Phys. Rev. B* **1993**, *47*, 558.
- (33) Kresse, G.; Hafner, J. *Phys. Rev. B* **1994**, *49*, 251.
- (34) Kresse, G.; Furthmüller, J. *Phys. Rev. B* **1996**, *54*, 11169.
- (35) Kresse, G.; Furthmüller, J. *Comput. Mater. Sci.* **1996**, *6*, 15.
- (36) Blöchl, P. E. *Phys. Rev. B* **1994**, *50*, 17953.
- (37) Kresse, G.; Joubert, D. *Phys. Rev. B* **1999**, *59*, 1758.
- (38) Perdew, J. P.; Burke, K.; Ernzerhof, M. *Phys. Rev. Lett.* **1997**, *78*, 1396.
- (39) Wyckoff, R. W. G. *Crystal structures vol II*; John Wiley & Sons, 1963.
- (40) Monkhorst, H. J.; Pack, J. D. *Phys. Rev. B* **1976**, *13*, 5188.
- (41) Bockris, J. O.; Dandapani, B.; Cocke, D.; Ghoroghchian, J. *Int. J. Hydrogen Energy* **1985**, *10*, 179.
- (42) Rossmeisl, J.; Qu, Z. W.; Zhu, H.; J-Kroes, G.; Norskov, J. K. *J. Electroanal. Chem.* **2007**, *607*, 83.

- (43) Norskov, J.; Bligaard, T.; Logadottir, A.; Bahn, S.; Hansen, L. B.; Bollinger, M.; Bengaard, H.; Hammer, B.; Sljivancanin, Z.; Mavrikakis, M.; Xu, Y.; Dahl, S.; Jacobsen, C. *J. H. J. Catal.* **2002**, *209*, 275.
- (44) Hill, T. L. *An introduction to statistical thermodynamics*; Dover Publications Inc, 1960.
- (45) Kleiman-Shwarsstein, A.; Huda, M. N.; Walsh, A.; Yan, Y.; Stucky, G. D.; Hu, Y.; Al-Jassim, M. M.; McFarland, E. W. *Chem. Mater* **2010**, *22*, 510.
- (46) Pala, R. G. S.; Matiu, H. *J. Phys. Chem. C* **2007**, *111*, 8617.

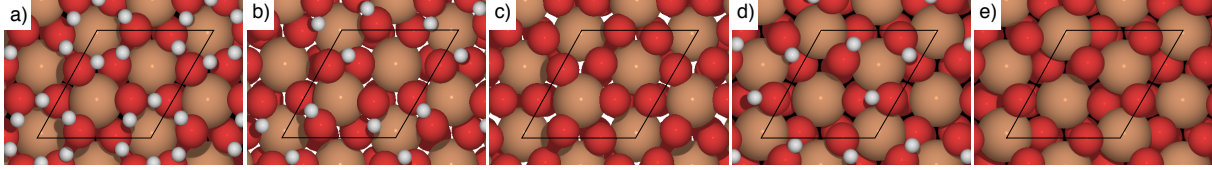


Figure 1: (Color online) The surface structure of the five considered terminations, i.e., $(\text{OH})_3\text{-Fe-H}_3\text{O}_3\text{-R}$, $(\text{OH})_3\text{-Fe-O}_3\text{-R}$, $\text{O}_3\text{-Fe-O}_3\text{-R}$, $(\text{OH})_3\text{-R}$ and $\text{O}_3\text{-R}$. The hydroxyl terminated surfaces form a hydrogen-bonded network. The 1×1 unitcell is shown as a solid line.

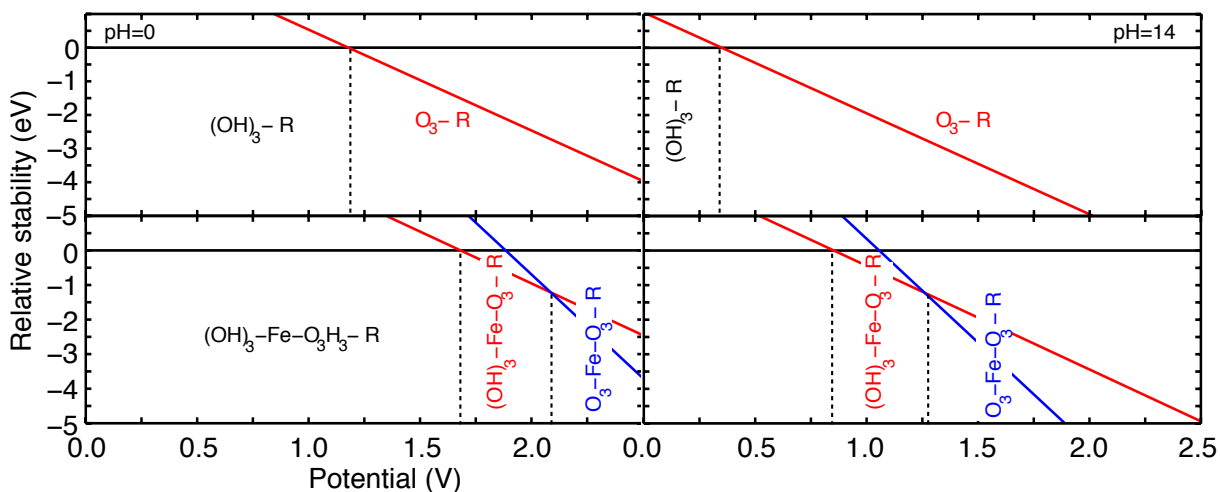


Figure 2: (Color online) The relative stability of all considered surface terminations as a function of applied potential and at two different pH, namely, pH=0 (left) and pH=14 (right). In the top figure, the $(\text{OH})_3\text{-R}$ (black) and $\text{O}_3\text{-R}$ (red) terminations are compared, whereas in bottom figure the $(\text{OH})_3\text{-Fe-O}_3\text{H}_3\text{-R}$ (black), $(\text{OH})_3\text{-Fe-O}_3\text{-R}$ (blue) and $\text{O}_3\text{-Fe-O}_3\text{-R}$ (red) terminations are compared.

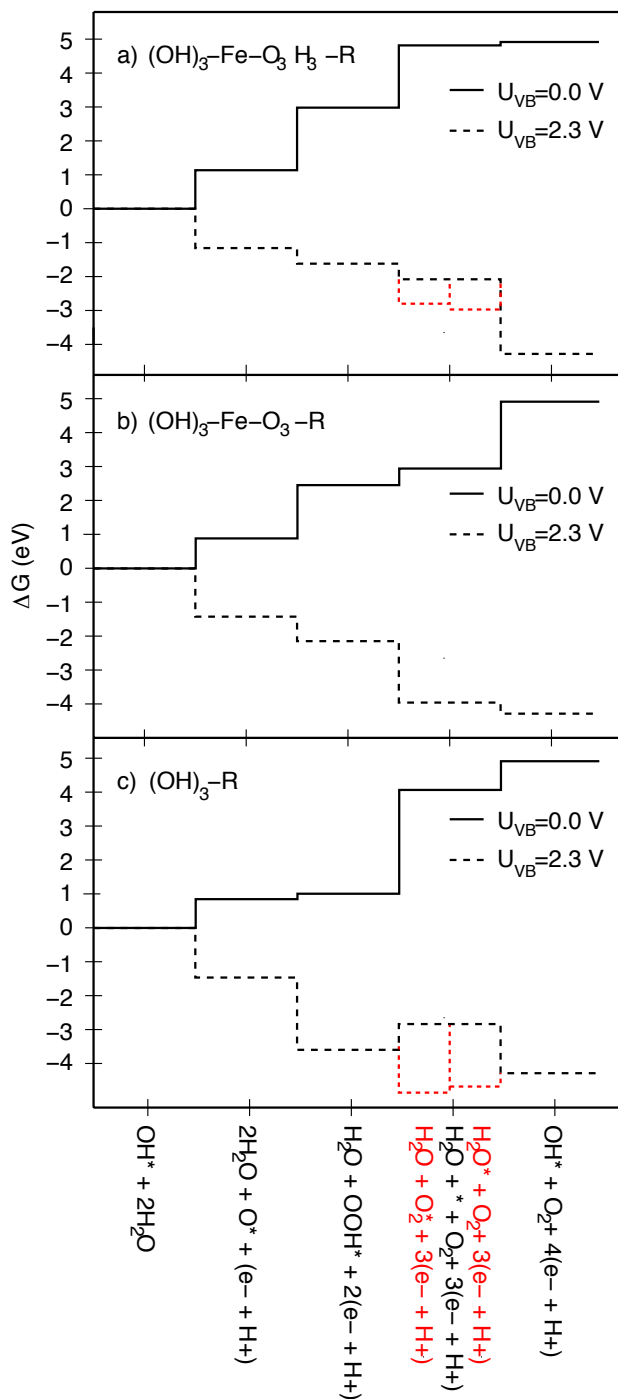


Figure 3: The free energies of reaction intermediates for different values of applied potential for a) $(\text{OH})_3\text{-Fe-O}_3\text{H}_3\text{-R}$, b) $(\text{OH})_3\text{-Fe-O}_3\text{-R}$ and c) $(\text{OH})_3\text{-R}$ surface terminations. At the corresponding value of the redox potential versus normal hydrogen electrode (NHE) for the photo-induced holes ($U_{VB}=2.3$ eV), all reaction steps are downhill and the photo-oxidation can proceed spontaneously, at least from a thermodynamic perspective. For $(\text{OH})_3\text{-R}$ the formation of O_2 is thermodynamically uphill and can be considered the rate-limiting step. Red lines represent non-electrochemical steps (see text).

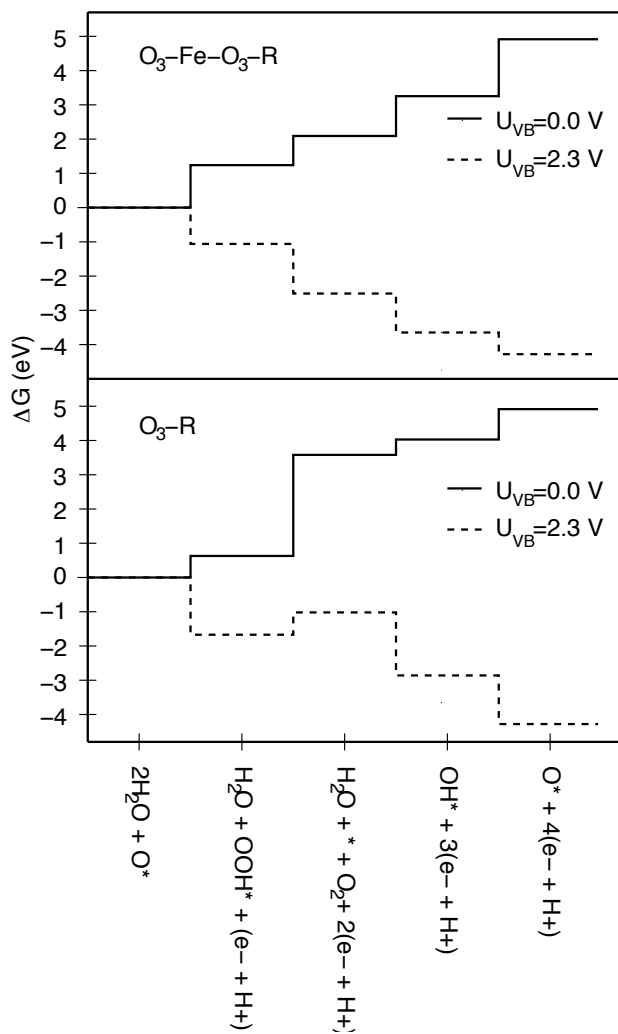


Figure 4: The free energies of reaction intermediates for different values of applied potential for the $\text{O}_3\text{-Fe-O}_3\text{-R}$ and $\text{O}_3\text{-R}$ surface terminations. At the corresponding value of the redox potential versus NHE for the photo-induced holes ($U_{\text{VB}} = 2.3 \text{ eV}$), all reaction steps on $\text{O}_3\text{-Fe-O}_3\text{-R}$ are downhill and the photo-oxidation can proceed spontaneously, at least from a thermodynamic perspective. However, on $\text{O}_3\text{-R}$, the formation of O_2 is thermodynamically uphill and can be considered as the rate-limiting step.

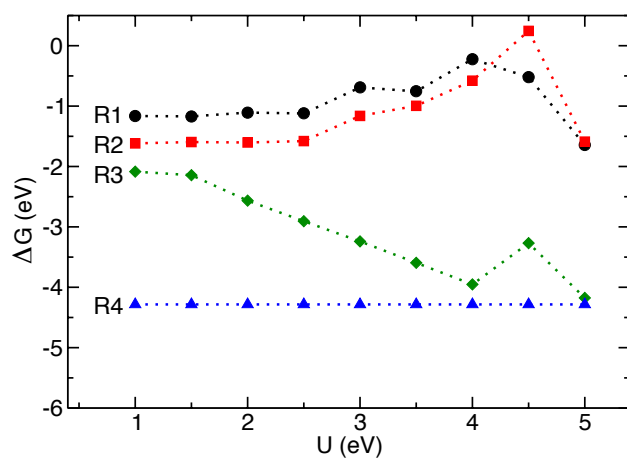


Figure 5: The free energies of reactions R1-R4 on the $(\text{OH})_3\text{-Fe-O}_3\text{H}_3\text{-R}$ termination as a function of the on-site Coulomb repulsion. Black circles denote R1, red squares denote R2, green diamonds denote R3, and finally blue triangles denote R4.